Using distributed temperature sensing (DTS) for locating and characterising infiltration and inflow into foul sewers before, during and after snowmelt period

Panasiuk, Oleksandr; Hedström, Annelie; Langeveld, Jeroen; de Haan, Cornelis; Liefting, Erik; Schilperoort, Remy; Viklander, Maria

DOI
10.3390/w11081529

Publication date
2019

Document Version
Final published version

Published in
Water (Switzerland)

water

MDPI

Article

Using Distributed Temperature Sensing (DTS) for Locating and Characterising Infiltration and Inflow into Foul Sewers before, during and after Snowmelt Period

Oleksandr Panasiuk [1,*], Annelie Hedström [1], Jeroen Langeveld [2,3], Cornelis de Haan [3], Erik Liefting [3], Remy Schilperoort [3] and Maria Viklander [1]

1 Department of Civil, Environmental and Natural Resources Engineering, Luleå University of Technology, 971 87 Luleå, Sweden
2 Department of Water Management, TU Delft, 2628 CN Delft, The Netherlands
3 Partners4UrbanWater, 6532 ZV Nijmegen, The Netherlands
* Correspondence: oleksandr.panasiuk@ltu.se

Received: 13 June 2019; Accepted: 23 July 2019; Published: 24 July 2019

Abstract: Infiltration and inflow (I/I) into sewers cause negative effects on the sewer system, wastewater treatment plant and environment. Identifying the causes and locating the inflows is necessary in order to address the I/I problem. This paper focuses on using distributed temperature sensing (DTS) for identifying, locating and characterising I/I into a sewer system during the end of winter–beginning of summer transition period under dry and wet weather conditions. During snowmelt, several locations with I/I were identified, while these locations did not show I/I during storm events after the snowmelt. In addition, during a very heavy storm after the snowmelt period, I/I was found at other locations. Therefore, DTS was demonstrated to be effective in identifying the type of I/I and in locating I/I. Finally, I/I monitoring campaigns in cold climates should take into account the variety of pathways of I/I during snowmelt and during rainfall.

Keywords: distributed temperature sensing; infiltration and inflow; snowmelt; foul sewers

1. Introduction

Infiltration and inflow (I/I) into foul and combined sewers have a number of negative effects on both the sewer system and the wastewater treatment plant (WWTP), including reduced effective capacity of sewers, increased risk of flooding and sanitary sewer overflows, increased hydraulic load on WWTP and reduced efficiency of wastewater treatment, accelerated deterioration of the system and increased costs of operation [1–3].

The causes of I/I may include the water entering the sewers through broken pipes, poor pipe connections, manholes, roof and basement drains [4,5]. Infiltration typically consists of water—mostly groundwater but also rainwater—that enters the sewers from the surrounding soil, while inflows typically occur during storm events via wrongly connected impervious surfaces.

Mattsson et al. [6] reported levels of dilution of wastewater by I/I from catchments with both mainly separate and mainly combined sewer systems as well as at the inflow to WWTP (approximately 700,000 PE (person equivalent), south Sweden) of around 1.6–2.2 times for the dry period, and from 1.6 up to 8.2 times during the wet weather period. The average I/I share of total influent wastewater to ten big WWTPs in Sweden was around 46% in 2015 with the average share of separate sewers around 80–85%, and 41% in Finland with a 95% share of separate sewer systems [7]. The average I/I rate into sewers in Germany has been estimated at 25% of the total flow. Rödel et al. [8] have also reported

increased I/I rates into 100,000 PE WWTP due to increased rainfall amounts (almost tripling in May as compared to January). Kaczor and Bugajski [9] studied I/I rates during snowmelt into five small-scale WWTPs in Poland (<2000 PE) and found that 43% to 70% of their daily inflows was I/I.

Measurements of I/I rate can improve strategies for sewer rehabilitation [4] and the locations of the inflows should be identified in order to remove the sources of I/I [10]. A number of methods have been developed for the detection of I/I, including those based on comparison of the reference flow (e.g., night flow, debited water by drinking water plant, etc.) with the measured flow (e.g., from monitored subcatchment, at the inflow point to WWTP, etc.) or based on commonly used wastewater quality parameters (e.g., nutrients, conductivity, etc.) [6,11–14]. The main drawback of these methods is their low capability to identify I/I locations, which is a prerequisite for being able to remove them. One method that could potentially be used to both detect and locate I/I is distributed temperature sensing (DTS) [10,14].

DTS is based on analysing the Raman backscattering of reflected laser impulses sent into a fibre-optic cable and described in more detail by Hoes et al. [15]. Previous studies on DTS application in sewers have focused on finding illicit wastewater connections to stormwater sewers [15], monitoring combined sewers [16] and detecting stormwater inflows into wastewater systems [10]. These previous studies have suggested that DTS is effective in detecting anomalies in the temperature dynamics in sewers. As I/I also often influences the temperature profile in the sewer, DTS is a potentially effective method for detecting and locating I/I [17], as well as distinguishing the pathways of I/I into sewers.

During the snowmelt period, which is of special importance in cold climate regions such as Scandinavia, Canada and northern USA [4,5,18–20], snowmelt may cause snowmelt-induced I/I. Snowmelt saturates the soil for a longer period of time as compared to rain events, especially in city environments, where the higher daily melting rate as compared to rural areas [21] makes snowmelt an important factor that contributes to I/I into sewers. There has been no scientific study published evaluating DTS technology for I/I detection in connection with the snowmelt period.

Managing I/I in sewers requires that the causes (and location) of the I/I are known. Consequently, there is a need to be able to distinguish between the different pathways of I/I: continuous infiltration of groundwater into the sewer (CI), rainfall runoff-caused inflow due to direct runoff (RRI), rainfall-induced infiltration due to temporally increasing groundwater tables after storm events (RGI), snowmelt-induced inflow due to runoff of melted snow (SRI) or snowmelt-induced infiltration due to increasing groundwater tables due to snowmelt (SGI).

This paper focused on how information from DTS can be used to characterise I/I in order to determine the pathways of I/I, what are the differences in the pathways before, during and after the snowmelt period (the end of winter–beginning of summer transition period), under dry and wet weather conditions, as well as how effective is DTS in identifying and locating the I/I into the sewers. Quantification of I/I requires flow measurements of wastewater [17] and was not part of this study.

2. Materials and Methods

2.1. Study Area

A field study was performed in the village with a population of 416 inhabitants in 2015 [22] within Skellefteå municipality, Sweden. The whole area was connected to a foul sewer system, while stormwater was managed mostly in open systems with swales.

The wastewater from an upstream area with 543 inhabitants in 2015 [22] was transported to the main sewer of the study area (thicker green and blue lines in Figure 1 from P8A to P3A). The main sewer system comprised an upstream pumping station P8A, a 193 m-long pressurised main (dotted grey line), 2315 m of gravity sewers and a downstream pumping station P3A (Figure 1).

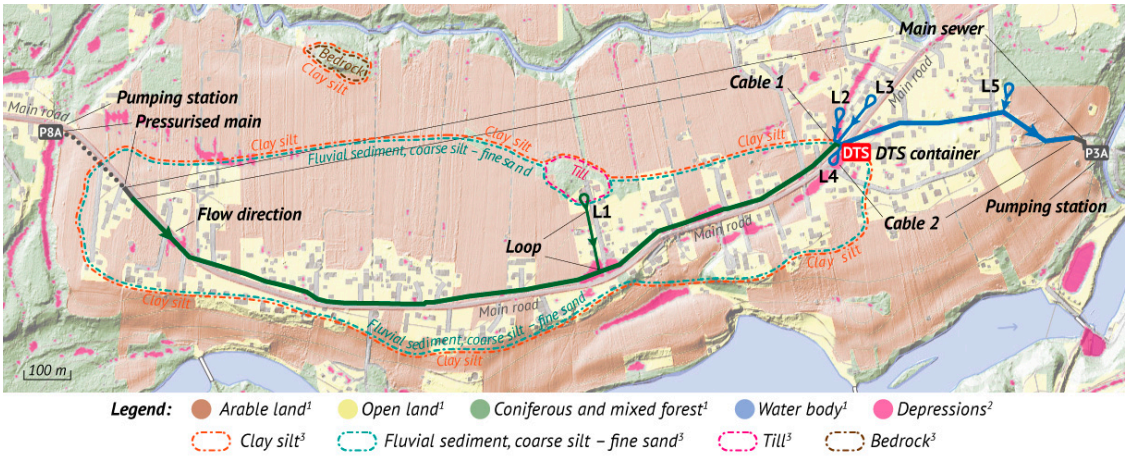

Figure 1. Map of the study area with a diagrammatic plan of the two distributed temperature sensing (DTS) cables installed in the sewer section between pumping stations P8A and P3A, connected to the DTS unit installed in the DTS container. Loops of the DTS cables are marked L1–L5. Sources for the information layers on the background map: [1] Topography maps from Lantmäteriet [23], [2] Depressions analysis by SCALGO Live [24] based on GSD-elevation data, Grid 2+ [23], [3] Soil map from Geological Survey of Sweden [25].

Predominantly, the land in the study area was used for agriculture (arable land), followed by spaces around buildings along the main sewer section (open land) and minor plots of coniferous and mixed forest that are located mainly along two rivers flowing northward and southward of the study area (Figure 1). Dominant soil types are fluvial sediment (coarse silt–fine sand) in the centre part of study area, surrounded by clay silt. Cable 1 is located in sewers lying fully in fluvial sediment soil, while cable 2 (except loop L4) is located in pipes lying in clay silt. In addition, minor regions of bedrock (northwest of the study area) and till (covering the north end of loop L1) are present in the study area (Figure 1).

The main road through the village (following the main sewer from P8A to DTS container, then continuing in the direction of loop L3 on Figure 1) divides the study area into two hydrological subcatchments: north and south. The receiving waters for the north catchment are a smaller river northwards from the study area, and for the south catchment, a bigger river southwards from the study area. Therefore, water from the bedrock area does not contribute to the I/I into sewers in the study area.

The study area was suggested by the municipality based on the flow monitoring results provided by a consultancy company during autumn 2013 and spring 2014. The conclusion was that the sewer section between pumping stations P8A and P3A is strongly affected by I/I.

2.2. Pathways of I/I

As mentioned above, there are a number of pathways for I/I into foul sewers (Figure 2). The continuous infiltration of groundwater into the sewer (CI) occurs over prolonged period of time through cracks in the pipes and loose pipe joints. Other examples of continuous infiltration include drinking water leakages and intrusion of water from receiving waters if the foul sewers are located near the shoreline [26]. As a direct response to rainfall for most types of storm events, rainfall runoff-caused inflow due to direct runoff (RRI) might occur. Inflows through manhole covers, through cross-connections between stormwater sewers and from wrongly connected roofs are usual pathways for RRI. Similar to RRI is snowmelt-induced inflow due to runoff of melted snow (SRI) as a direct response to snowmelt days. Finally, rainfall- (RGI) or snowmelt- (SGI) induced infiltration due to temporally increasing groundwater tables after heavier and longer rainfall events or during snowmelt periods can cause I/I into foul sewers (Figure 2).

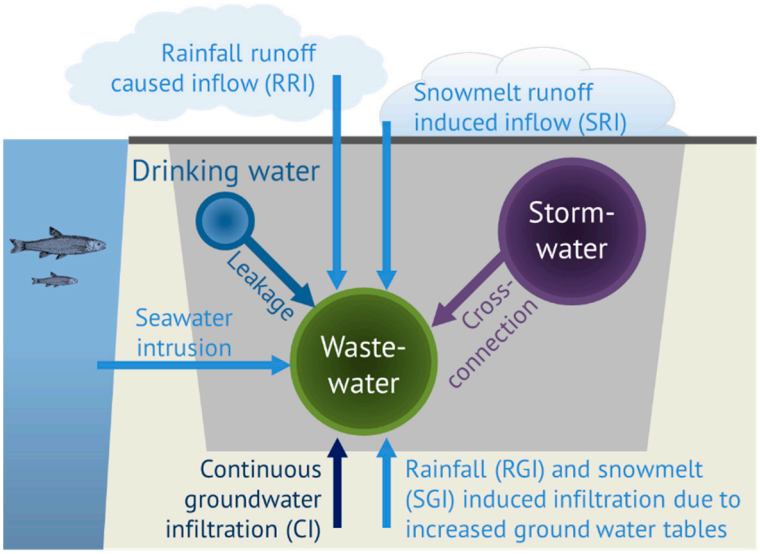

Figure 2. Pathways of I/I into foul sewers.

The absence of a traditional stormwater system, distance between foul sewers and drinking water pipes, and distance from the receiving waters in the study area excluded cross-connections, drinking water leakages and intrusion of water bodies from the analysis.

2.3. Experimental Setup and Instrumentation

The DTS monitoring campaign took place between 20 March (with the snow cover still present on the ground) and 23 June 2015.

Two fibre-optic cables, type MultiMode 50/125 µm–OM2/OM3 class, with lengths of 2050 m (cable 1) and 1225 m (cable 2), were installed at the invert of the gravity foul sewer, covering around 2180 m of the main sewer (Figure 1). Five tributary sewer pipes, L1–L5, with a total length of 355 m, were additionally selected for the DTS measurements (Figure 1). In all five tributary pipes, the fibre-optic cable was installed in the form of loop, so that the cable ran twice (upstream and downstream) along these pipes. Finally, around 60 m of cable 1 and 325 m of cable 2 were kept in manholes at different locations along the study site to provide spare length in case of cable damage. Both cables were connected to the DTS unit—XT-DTS (Silixa Ltd, London, UK)—using Multimode E2000/APC8 connectors (Silixa Ltd, London, UK). The DTS unit was installed inside the heated DTS container (Figure 1). For more details concerning installation setup, see Hoes et al. [15].

The time and space resolutions of the DTS measurements were around 14 s and 0.25 m. According to the product specifications [24], the temperature resolution was 0.01 °C; however, the actual temperature precision in this study was estimated to be around 0.1 °C due to instrumental noise.

Precipitation measurements before 30 April were performed using a Geonor T-200B weighting bucket rain gauge (Campbell Scientific, Edmonton, AB, Canada) with 0.2 mm accuracy installed 2.6 km ENE from the DTS unit. After that time, a MJK Meteorological tipping bucket rain gauge (MJK Automation, Säffle, Sweden) with a collection area of 200 cm^2 and resolution of 0.2 mm per pulse was used. Air temperature was measured every 30 s using a MicroLite USB temperature logger (fourtec Ltd, Burlington, MA, USA) with accuracy of around 0.03 °C. Both the tipping bucket and the temperature logger were installed outside the building of the downstream pumping station P3A, 0.5 km east of the DTS unit. Rain events in this study were considered to be separate if they had at least a 3 h dry period between each other. Figure 3 shows averaged air temperature and accumulated precipitation intensity for each hour.

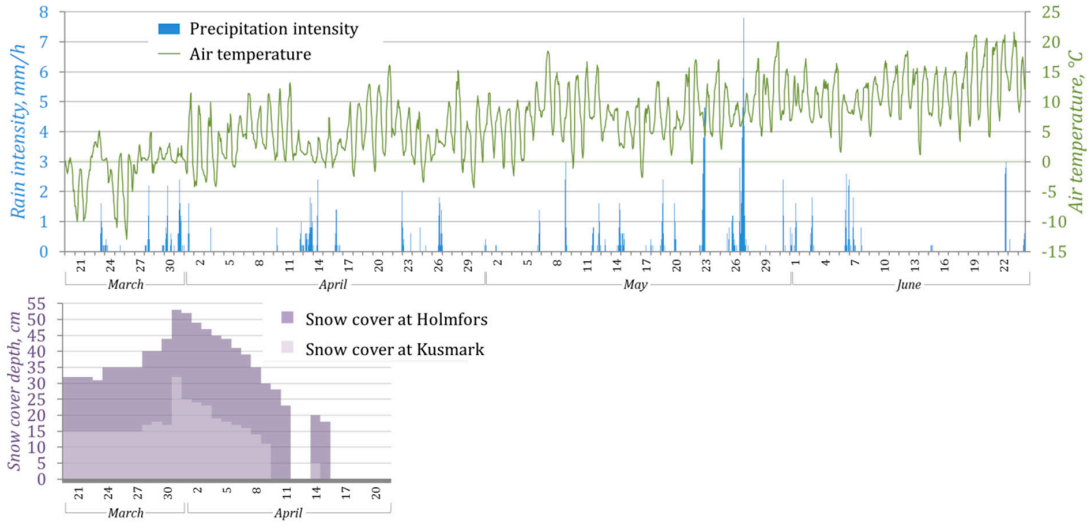

Figure 3. Weather data from the study site during the monitoring campaign. **Top**: precipitation intensity and air temperature. **Bottom**: snow cover depth at Holmfors and Kusmark weather stations.

Daily snow cover depth measurements with 1 cm resolution were obtained from the Swedish Meteorological and Hydrological Institute [25] from Kusmark and Holmfors stations, 14.6 km NNW and 16.4 km WNW from the DTS unit in the study area, respectively.

2.4. Data Processing

The raw data from the DTS unit were exported into csv-files by DTS Viewer Lite software (Release 4.0.4, Silixa Ltd). Using scripts in MATLAB R2016b (MathWorks, Natick, MA, USA), the temperature readings were averaged to uniform time and length steps and presented in the form of colour-coded plots (Figure 4). Time and location are represented by the vertical and horizontal axes, respectively, with one pixel on the plot covering 0.25 cm of spatial resolution and 30 s of temporal resolution. The colour of each pixel represents measured temperature.

Figure 4a,c shows the processed data collected with cable 1 (see also Figure 1) that was installed from the DTS unit in the upstream direction, thus the flow direction in the main sewer is from right to left on the plot. Plots for cable 2 have a flow direction in the main sewer from left to right (Figure 4b,d). The parts of both plots with central symmetry represent the parts of the cable installed in the tributary inflow pipes in the form of loops (Figure 4). Temperature anomalies in this study were determined by trained professionals as changes in temperature profile on DTS plots that were not caused by daily variations of wastewater temperature or inflows of wastewater into sewers.

Precipitation and air temperature measurements were recalculated as average hourly values for plotting.

Minitab 17 Statistical Software (Minitab, LLC, State College, PA, USA) and Microsoft Office Excel were used for the precipitation, snow depth and air temperature data analyses.

2.5. Localisation of Cable in Sewers

In order to match the distances on the DTS plots to the actual locations of the cable in the sewers, the following procedure was undertaken on 16 and 17 June 2015. Down in the manhole, the DTS cable was lifted from the water, and freeze spray containing 95–100% 1,1,1,2-tetrafluoroethane was applied to the cable for 30–120 s. Subsequently, raw data from the DTS unit (data before DTS plots visualisation in Matlab) was analysed: the cable distance where the temperature dropped the most due to the freezing corresponded to the location where the spray was applied. In total, 28 locations were treated in this way. The distances in between these reference points were calculated using GIS maps provided by the municipality.

3. Results

3.1. Snow Cover Depth and Precipitation Volume

Observations at the beginning of the monitoring campaign on 20 March showed the snow cover depth was 15 cm and 32 cm at Kusmark and Holmfors stations, respectively, and after several snowfalls reached its maximum of 32 cm and 53 cm on 31 March (see Figure 3). Subsequently, the snow started to melt, with the highest melting rate on 9 April at Kusmark and 11 April at Holmfors, when all remaining snow depth of 11 cm and 23 cm, respectively, melted during one day. Another 12.8 mm of snowfall on 13 April resulted in a new 5 cm and 20 cm of snow cover observed the next day, and was completely melted on 14 April and 15 April at Kusmark and Holmfors, respectively. From 16 April, no snow cover was observed in the study area (Figure 3).

In total, 28 rain events occurred during the monitoring campaign (between 20 March and 23 June) with rain depths of 2 mm or more. For 14 of these rain events, a rain depth of 5 mm or higher was recorded. Table 1 presents the summary of these 14 rain events.

The rain events #9 and #11 occurred in the end of May, and had the highest rain depth of 23.6 mm and 41.4 mm, respectively. The highest average rain intensities were measured for the rain events #14, #9, #11 and #6 with 3.51 mm, 3.01 mm, 2.52 mm and 2.03 mm/h, respectively.

Table 1. Summary of the rain events during the monitoring campaign with a rain depth of 5 mm or higher.

Event No.	Start		End		Duration, h:min	Rain Depth, mm	Average Intensity, mm/h
	Date (Month-Day)	Time	Date (Month-Day)	Time			
1	03-28	06:45	03-28	11:18	04:33	5.6	1.23
2 *	03-30	01:36	03-30	07:52	06:16	5.8	0.93
3 *	03-31	06:56	03-31	18:18	11:22	11.6	1.02
4	04-13	04:08	04-13	23:03	18:55	12.8	0.68
5	04-26	11:32	04-26	22:16	10:44	8.8	0.82
6	05-09	09:06	05-09	12:15	03:09	6.4	2.03
7	05-14	15:12	05-14	23:06	07:54	5.2	0.66
8	05-19	00:30	05-19	08:07	07:37	7.0	0.92
9	05-23	02:42	05-23	10:32	07:50	23.6	3.01
10	05-26	02:03	05-26	09:35	07:32	5.2	0.69
11 *	05-26	20:06	05-27	12:32	16:26	41.4	2.52
12	06-06	11:59	06-06	15:43	03:44	6.2	1.66
13	06-06	18:47	06-06	22:14	03:27	5.4	1.57
14	06-22	14:42	06-22	17:09	02:27	8.6	3.51

* Events detected by DTS.

3.2. DTS Results

The snowmelt period resulted in temperature anomalies on the DTS plots, as did two out of four rain events that occurred when a snow cover still was present. In spring, when the snow cover was gone, temperature anomalies on the DTS plots were detected for the largest rain event (out of 10 events), indicating I/I into the foul sewers.

3.2.1. Rain during Snow Cover Presence

Two rain events (#2 and #3), when the snow cover was still present in the area, may have been detected as temperature anomalies in the foul sewer. Temperature anomalies were detected on the DTS plots with a starting point of approximately 30 March at 11:00 for cable 1 (Figure 4a) and at 13:00 for cable 2 (Figure 4b), and were interpreted as an infiltration of colder water related to the rain event #2 (see Table 1). These temperature anomalies continued until approximately 20:00 on 31 March (Figure 4a), coinciding with the rain event #3 (Table 1), and were also interpreted as rain infiltration.

Six temperature anomalies were located for cable 1 and two for cable 2 during the two abovementioned rain events during the presence of snow cover (Table 2). Site descriptions of these temperature anomalies revealed by the localisation analysis of the actual cable position in the sewers relative to the distance on the x-axis of the DTS plots are summarised in Table 1. With the

exception of the 663 m location (cable 1), none of the locations for the rain-on-snow events had tributary inflows in their proximity.

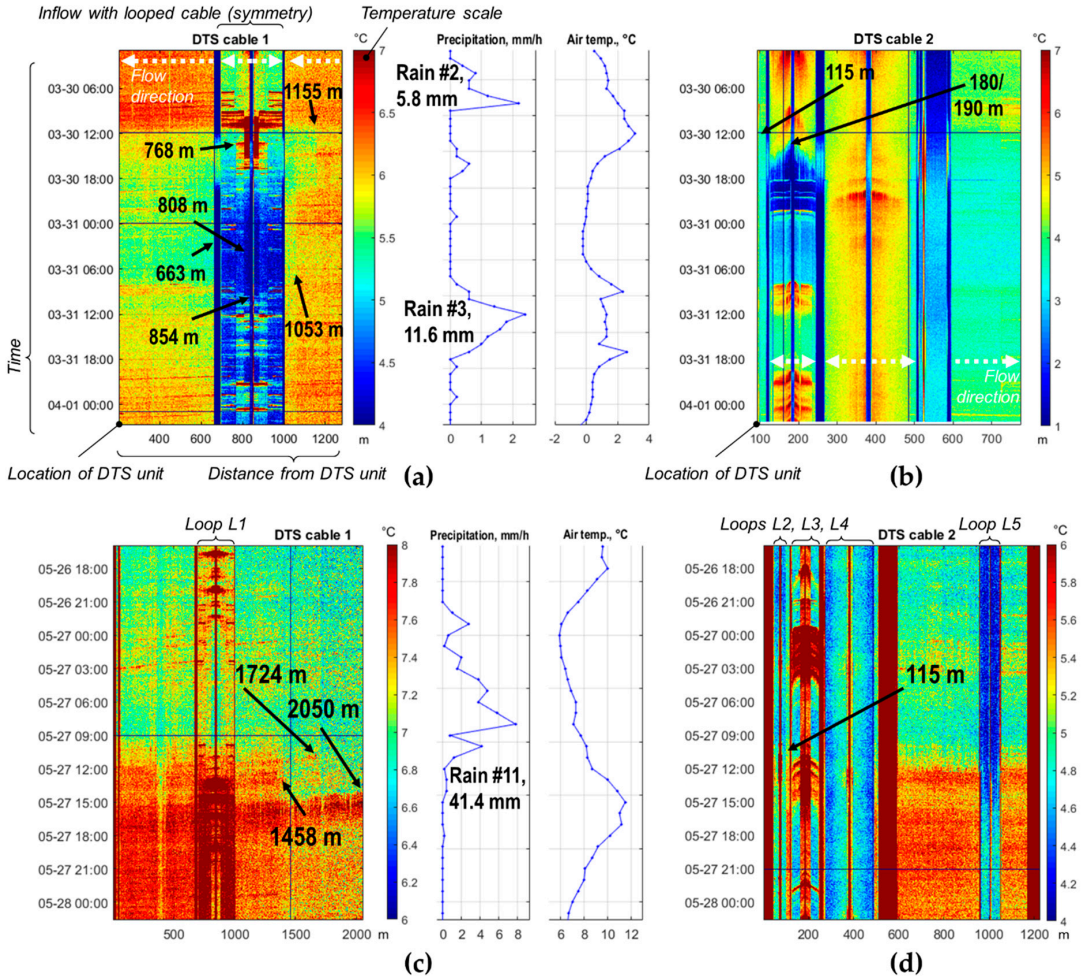

Figure 4. The DTS plot for cable 1 (**a**,**c**) and cable 2 (**b**,**d**) with identified temperature anomalies (solid line arrows) during rain events #2 and #3 (**a**,**b**) and #11 (**c**,**d**) visible. Note the difference in the temperature scales.

Table 2. Summary of identified temperature anomalies (marked with plus sign) during rain-on-snow, snowmelt and rain events and their possible pathways (UI—upstream inflow) (discussed further in the discussion section). RGI/SGI—rainfall/snowmelt induced groundwater infiltration; SRI—snowmelt runoff inflow; UI—upstream inflow.

Cable	Location along Cable, m	Site Description	Detected Temperature Anomalies			Possible Pathways
			Rain-on-Snow	Snowmelt	Rain Events	
1	663	Downstream end of tributary pipe L1	+	+		SGI/UI
1	768	In the middle of tributary pipe L1	+	+		SGI
1	808	In the middle of tributary pipe L1	+	+		SGI
1	854	Upstream end of tributary pipe L1	+	+		SGI
1	1053	In a manhole	+	+		SGI/SRI
1	1155	Between two manholes on the main sewer section	+	+		SGI
1	1458	Between two manholes with the lateral connections from private properties nearby			+	RGI
1	1724	Between two manholes with the lateral connections from private properties nearby			+	RGI
1	2050	Upstream end of the main sewer			+	UI
2	115	Inflow from upstream main sewer	+	+	+	UI
2	180/190	Upstream end of tributary pipe L3	+	+		SGI

3.2.2. Snowmelt Period

According to the observations of snow depth at Kusmark and Holmfors stations, the snow started to melt on 31 March with maximum snowmelt intensity reached on 9 and 11 April, respectively. The first visible temperature anomaly interpreted as inflow of colder water on the DTS plots was on 5 April afternoon, becoming clearer and more intensive from 6 April afternoon.

The identified locations of temperature anomalies from snowmelt for both cable 1 and cable 2 were the same as for the rain events #2 and #3 when the snow cover was still present (Table 2). These temperature anomalies were not visible after 20 April for cable 1, and after 21 April for cable 2.

3.2.3. Rainfall Inflow

After the snow was completely melted on 16 April, ten rainfall events with a rain depth of 5 mm or higher occurred in the study area. One of these ten rain events, the largest rain event #11 (26 May), with a rain depth of 41.4 mm, resulted in a temperature increase on the DTS plots (Figure 4c,d). This increase was detected in the form of three temperature anomalies along cable 1 and one temperature anomaly along cable 2 (Table 2).

4. Discussion

The results from the DTS measurements (Figure 4 and Table 2) and the following analyses revealed a number of temperature anomalies that can be associated with the I/I problem in the sewer section of the study area during the end of winter–beginning of summer transition period.

As mentioned above, prior to the DTS monitoring campaign, the following pathways of I/I entering foul sewers were identified: continuous groundwater infiltration (CI), rainfall and snowmelt runoff inflow (RRI and SRI), and rainfall- (RGI) or snowmelt- (SGI) induced infiltration due to temporally increasing ground water tables. Combining information from the localisation of temperature anomalies (Table 2) with the weather data (temperature, precipitation intensity and snow cover depth) (Figure 3) made it possible to distinguish these pathways in this study.

The events described as rainfall during snow cover presence indicated the same ingression points of I/I as those during snowmelt induced by higher air temperature (Table 2). Rains on snow have been reported to result in higher flow as compared to similar rains after the snowmelt period [21], which can explain why rain events #2 and #3 were detected by DTS. Due to the water storage capacity of the snow [27], the rain-on-snow event without snowmelt (#1) possibly did not reach sewers and therefore was not visible on the DTS plots, suggesting no RRI. It is therefore concluded that the most probable pathway for I/I during both snowmelt period and rain events #2 and #3 is SGI. In one case, a temperature anomaly was located in a manhole (1053 m, cable 1), suggesting an additional possible pathway in form of SRI.

No temperature anomalies related to smaller rain events after the snow cover had disappeared (after 16 April) were observed on the DTS plots. This suggests that the sewer section in the study area had no wrongly connected roofs directly connected to the sewers. This finding was consistent with the municipality's own dye tests carried out in the study area the year before the DTS monitoring campaign. Additionally, all identified locations of temperature anomalies during the rain events after snowmelt had no manholes in their proximity (Table 2), which excludes direct inflow through manhole covers. These two findings suggest no RRI for the smaller rain events.

A study focused on the detection limits of DTS [28] found that due to the noise of the measurements, direct inflows with smaller volumes and higher temperature differences were more difficult to detect than inflows with larger volumes and smaller temperature differences. The temperature of I/I is affected by a number of factors such as air, soil, ground surface and roof temperature as well as the length of tributary pipes [28,29]. Even within the duration of the shortest rain event (#14) of 2.45 h, the air temperature changed from 21.2 °C to 14.9 °C, while the wastewater temperature was relatively stable: 7.6 ± 0.2 °C in the upstream end and 8.4 ± 0.2 °C in the downstream end of the main sewer section. Therefore, it is unlikely that the temperature differences between wastewater and I/I in the form of RRI were below the noise level of DTS during the whole rain event.

Since only the largest rain event #11 resulted in temperature anomalies on the DTS plots and no sources of direct inflow from the roofs were identified with the dye testing, the infiltration due to the elevated groundwater level (RGI) or percolating water is suspected to have generated I/I during the rain event #11.

The temperature anomalies from rain event #11 (Figure 4, bottom) were found at different locations compared to the snowmelt-induced temperature anomalies, which could be explained by the presence of the snow cover affecting the surface runoff, saturated soil with minimised infiltration capacity [21] and frozen soil affecting in-soil water paths [30]. Therefore, for I/I monitoring campaigns, it is important to keep in mind that locations where no I/I problems were detected during snowmelt period might still have I/I after snow has melted, and vice versa.

Excluding temperature anomalies due to upstream inflow (Table 2), out of nine identified I/I locations one was located in clay silt soil (end of the L3 loop), one in till (end of the L1 loop), and seven in the fluvial sediment (coarse silt–fine sand) (Figure 1). Due to the isolated location, no sewers were within proximity of bedrock in the study area. These types of soils have on average the following hydraulic conductivity (from lowest to highest): bedrock—below 2×10^{-10} m/s; clay silt—5×10^{-13} to 2×10^{-9} m/s; till—9×10^{-13} to 2×10^{-6} m/s; coarse silt–fine sand—8×10^{-7} to 8×10^{-4} m/s [31].

Finally, the analysis of the DTS results was unable to demonstrate either presence or absence of continuous groundwater infiltration (CI) or drinking water leakage into the foul sewers in the study area.

Additional Information from DTS Plots

Even when no temperature anomalies indicating I/I into the sewers were detected by DTS, it was possible to obtain additional information from the DTS plots: relative flow velocity and flow direction.

The gradients of the heat traces on the DTS plots (dx/dt) can provide information about the flow velocity [10]. For example, warmer inflows from the houses into the cable loop L3 (Figure 5, left) were shaped more horizontally (higher dx/dt) around noon, indicating faster velocity as compared to the inflows that occurred at night (lower dx/dt), as the result of higher flow in the sewers during the day compared to night time.

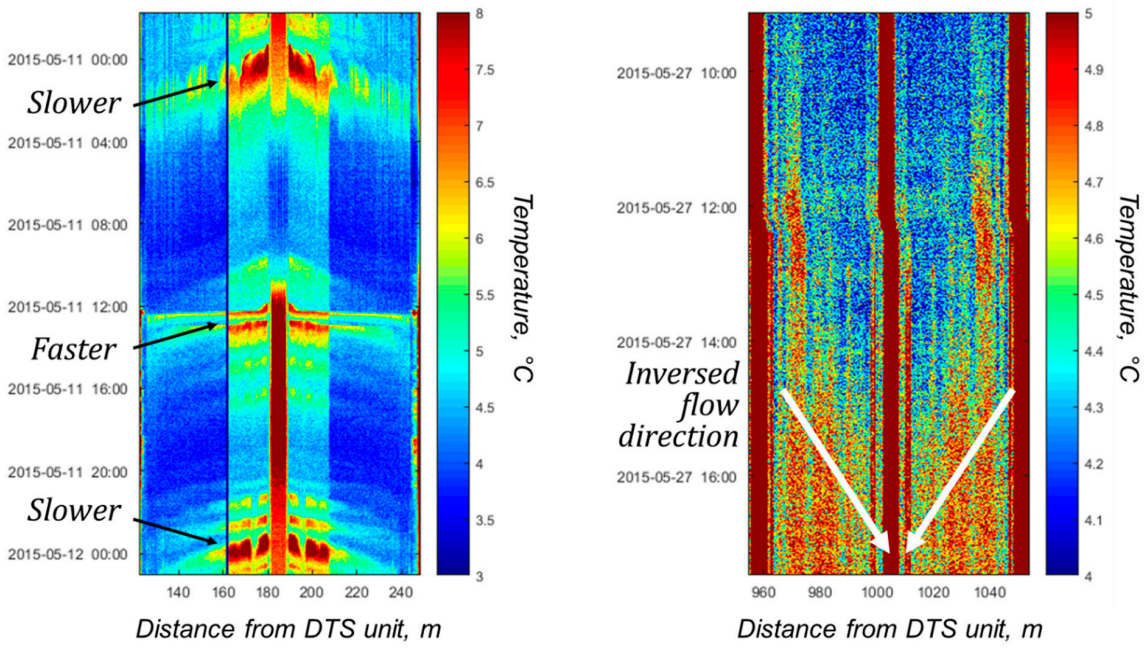

Figure 5. Additional information obtained from DTS plots: relative flow speed in loop L3 (**left**) and flow direction in loop L5 (**right**). Note different temperature scales.

Finally, the negative gradients of heat traces of warmer wastewater from the main sewer section can be observed inside the loop L5 at the end of the rain event #11 (Figure 5, right). This was a strong indication of the high water level in the main sewer section resulting in the inverse flow direction into the tributary sewer pipe.

5. Conclusions

It is concluded that due to the high temporal and spatial resolution as well as the measurements over a prolonged period of time (over three months), DTS has shown to be effective for identifying, locating and characterising the pathways of I/I into the system during the end of winter–beginning of summer transition period, under dry and wet weather conditions.

During the snowmelt period (around 13 days), temperature anomalies related to I/I were detected in seven locations along the study section using DTS. All of the locations except one had no tributary inflows in their proximity, which suggests SGI through poor pipe joints or leaking manholes as the most probable reasons for I/I. During rain-on-snow events, the DTS plots did not reveal any temperature anomalies unless the snowmelt was occurring due to higher air temperature at the same time. Those visible rain-on-snow events (#2 and #3) resulted in temperature anomalies in the same locations as the ones induced by the snowmelt events, and were concluded to also be SGI. One temperature anomaly located in a manhole might have an additional pathway in the form of SRI.

Ten rain events (#5–#14) occurred after the snow cover had melted completely and only the largest (#11) caused temperature anomalies that were visible on the DTS plots. The fact that smaller rains were not visible on the DTS plots suggests that no roofs in the area were wrongly connected to the foul sewers (no RRI). All of the temperature anomalies during rain #11 were at different locations from those during snowmelt and were concluded to be caused by RGI.

It is therefore recommended to perform the DTS monitoring campaign under different weather conditions, including snowmelt period and rains with different volumes, to be able to detect I/I occurring in different locations according to conditions.

Finally, additional information such as flow velocity and flow direction could be estimated from DTS plots. However, further studies are recommended in order to increase the accuracy of these measurements.

Author Contributions: This work was accomplished as a part of O.P.'s PhD studies under the supervision of A.H. and M.V. Visualisation and analysis of DTS data were performed by E.L., R.S., C.d.H., J.L and O.P. The design of the experimental setup and field measurements were performed by O.P. with valuable contributions from C.d.H. Data analysis and writing of the paper, were performed by O.P. together with valuable contributions and support from A.H. and M.V.

Funding: This work has been carried out with financial support from the Research Council Formas (2012-618), Vinnova (2011-03232) and Skellefteå municipality, within the Stormwater&Sewers (Dag&Nät) research cluster.

Acknowledgments: The authors thank Bo Hellgren and his colleagues from Skellefteå municipality for their valuable support in the field work.

Conflicts of Interest: The authors declare no conflict of interest.

References

1. Bareš, V.; Stránský, D.; Sýkora, P. Evaluation of sewer infiltration/inflow using COD mass flux method: Case study in Prague. *Water Sci. Technol.* **2012**, *66*, 673–680. [CrossRef] [PubMed]
2. Karpf, C.; Krebs, P. Quantification of groundwater infiltration and surface water inflows in urban sewer networks based on a multiple model approach. *Water Res.* **2011**, *45*, 3129–3136. [CrossRef] [PubMed]
3. Mattsson, A.; Nivert, G.; Heinonen, M. Direct precipitation on demand at large Scandinavian WWTPs reduces the effluent phosphorus load. *Water Sci. Technol.* **2012**, *65*, 2106–2111. [CrossRef] [PubMed]
4. Field, R.; O'Connor, T.P. Control strategy for storm-generated sanitary-sewer overflows. *J. Environ. Eng.* **1997**, *123*, 41–46. [CrossRef]

5. Staufer, P.; Scheidegger, A.; Rieckermann, J. Assessing the performance of sewer rehabilitation on the reduction of infiltration and inflow. *Water Res.* **2012**, *46*, 5185–5196. [CrossRef] [PubMed]
6. Mattsson, J.; Mattsson, A.; Davidsson, F.; Hedström, A.; Österlund, H.; Viklander, M. Normalization of Wastewater Quality to Estimate Infiltration/Inflow and Mass Flows of Metals. *J. Environ. Eng.* **2016**, *142*, 04016050. [CrossRef]
7. Jenssen Sola, K.; Bjerkholt, J.T.; Lindholm, O.G.; Ratnaweera, H. Infiltration and Inflow (I/I) to Wastewater Systems in Norway, Sweden, Denmark, and Finland. *Water* **2018**, *10*, 1696. [CrossRef]
8. Rödel, S.; Günthert, F.W.; Brüggemann, T. Investigating the impacts of extraneous water on wastewater treatment plants. *Water Sci. Technol.* **2017**, *75*, 847–855. [CrossRef]
9. Kaczor, G.; Bugajski, P. Impact of Snowmelt Inflow on Temperature of Sewage Discharged to Treatment Plants. *Pol. J. Environ. Stud.* **2012**, *21*, 381–386.
10. Schilperoort, R.; Hoppe, H.; de Haan, C.; Langeveld, J. Searching for storm water inflows in foul sewers using fibre-optic distributed temperature sensing. *Water Sci. Technol.* **2013**, *68*, 1723–1730. [CrossRef]
11. Cahoon, L.B.; Hanke, M.H. Rainfall effects on inflow and infiltration in wastewater treatment systems in a coastal plain region. *Water Sci. Technol. J. Int. Assoc. Water Pollut. Res.* **2017**, *75*, 1909–1921. [CrossRef] [PubMed]
12. De Bénédittis, J.; Bertrand-Krajewski, J.L. Infiltration in sewer systems: Comparison of measurement methods. *Water Sci. Technol.* **2005**, *52*, 219–227. [CrossRef]
13. Kracht, O.; Gujer, W. Quantification of infiltration into sewers based on time series of pollutant loads. *Sewer Process. Netw. IV* **2005**, *52*, 209–218. [CrossRef]
14. Panasiuk, O.; Hedström, A.; Marsalek, J.; Ashley, R.M.; Viklander, M. Contamination of stormwater by wastewater: A review of detection methods. *J. Environ. Manag.* **2015**, *152*, 241–250. [CrossRef] [PubMed]
15. Hoes, O.A.C.; Schilperoort, R.P.S.; Luxemburg, W.M.J.; Clemens, F.H.L.R.; van de Giesen, N.C. Locating illicit connections in storm water sewers using fiber-optic distributed temperature sensing. *Water Res.* **2009**, *43*, 5187–5197. [CrossRef] [PubMed]
16. Schilperoort, R.P.S.; Clemens, F.H.L.R. Fibre-optic distributed temperature sensing in combined sewer systems. *Water Sci. Technol.* **2009**, *60*, 1127–1134. [CrossRef] [PubMed]
17. Beheshti, M.; Sægrov, S. Detection of extraneous water ingress into the sewer system using tandem methods—A case study in Trondheim city. *Water Sci. Technol.* **2019**, *79*, 231–239. [CrossRef]
18. Valeo, C.; Ho, C.L.I. Modelling urban snowmelt runoff. *J. Hydrol.* **2004**, *299*, 237–251. [CrossRef]
19. Wittenberg, H.; Aksoy, H. Groundwater intrusion into leaky sewer systems. *Water Sci. Technol.* **2010**, *62*, 92–98. [CrossRef]
20. Wright, L.; Heany, J.; Dent, S. Prioritizing sanitary sewers for rehabilitation using least-cost classifiers. *J. Infrastruct. Syst.* **2006**, *12*, 174–183. [CrossRef]
21. Bengtsson, L.; Westerström, G. Urban snowmelt and runoff in northern Sweden. *Hydrol. Sci. J.* **1992**, *37*, 263–275. [CrossRef]
22. Statistiska Centralbyrån Befolkning i Tätorter 2015-12-31; Fördelat på kön och Åldersklasser. Available online: http://www.scb.se/MI0810 (accessed on 1 May 2017).
23. Lantmäteriet Lantmäteriet, the Swedish Mapping, Cadastral and Land Registration Authority. Available online: https://kso.etjanster.lantmateriet.se/ (accessed on 16 January 2019).
24. Silixa XT-DTS^{TM}, Silixa, London UK. Available online: https://silixa.com/products/xt-dts/ (accessed on 12 March 2019).
25. SMHI. SMHI Öppna Data|Meteorologiska Observationer. Available online: http://opendata-download-metobs.smhi.se/explore/ (accessed on 6 May 2017).
26. Hey, G.; Jönsson, K.; Mattsson, A. *The Impact of Infiltration and Inflow on Wastewater Treatment Plants: A Case Study in Sweden*; Report No. 6; Svenskt Vatten VA-teknik Sodra: Lund, Sweden, 2016.
27. Moghadas, S.; Leonhardt, G.; Marsalek, J.; Viklander, M. Modeling Urban Runoff from Rain-on-Snow Events with the U.S. EPA SWMM Model for Current and Future Climate Scenarios. *J. Cold Reg. Eng.* **2018**, *32*, 04017021. [CrossRef]
28. Nienhuis, J.; de Haan, C.; Langeveld, J.; Klootwijk, M.; Clemens, F. Assessment of detection limits of fiber-optic distributed temperature sensing for detection of illicit connections. *Water Sci. Technol. J. Int. Assoc. Water Pollut. Res.* **2013**, *67*, 2712–2718. [CrossRef] [PubMed]

29. Bense, V.F.; Read, T.; Verhoef, A. Using distributed temperature sensing to monitor field scale dynamics of ground surface temperature and related substrate heat flux. *Agric. For. Meteorol.* **2016**, *220*, 207–215. [CrossRef]
30. Semadeni-Davies, A. Urban Water Management vs. Climate Change: Impacts on Cold Region Waste Water Inflows. *Clim. Chang.* **2004**, *64*, 103–126. [CrossRef]
31. Freeze, A.; Cherry, J. *Groundwater*; Prentice-Hall Inc.: Englewood Cliffs, NJ, USA, 1979; pp. 26–30.